A long-term comparison of nighttime cluster events and daytime ion formation in a boreal forest

Stephany Buenrostro Mazon*, Jenni Kontkanen, Hanna E. Manninen, Tuomo Nieminen, Veli-Matti Kerminen and Markku Kulmala

Department of Physics, P.O. Box 64, FI-00014 University of Helsinki, Finland (corresponding author's e-mail: stephany.mazon@helsinki.fi)

New particle formation (NPF) events are typically observed during daytime when photochemical oxidation takes place. However, nighttime nucleation mode particles have been observed across various locations only sporadically. We present 11 years (2003–2013) of air ion number size distribution data from the SMEAR II station in Hyytiälä, Finland, where during a third of the nights a sub-3 nm negative (n = 1324 days) and positive (n = 1174 days) ion events took place. To investigate nocturnal clustering at sizes above the constant small ion pool, we defined cluster events (CE) as a nocturnal event with 2–3 nm ion concentrations reaching $\geq$ 70 cm^{-3} between 18:00 and 24:00 local time. CE (n = 221 days) were characterized by a rapid, 10-fold increase in the median 2–3 nm ion concentration from the start (~10 cm^{-3}) to the event peak (~100 cm^{-3}). Furthermore, small and intermediate ions during the CE, NPF events and nonevents were compared: while concentrations of 1.5–2 nm ions were the highest during CE (median 235 cm^{-3}), as compared with the NPF events (96 cm^{-3}) or the daytime and nighttime nonevents (~20 cm^{-3}), 3–7 nm ion concentrations increased notably only during NPF events (median 52 cm^{-3}). Specifically, ion concentrations during CE decreased for sizes above ~2.4 nm (< 10 cm^{-3}). In addition, 90% of CE proceeded either a NPF event (55%) or a undefined day (35%), and only 10% of them proceeded a daytime non-event. This study suggests a build-up of 0.9–2.4 nm ion clusters during CE nights (18:00–24:00) that equals or exceeds the ion concentration levels during daytime NPF, but unlike the latter, CE fail to activate and grow clusters > 3 nm in diameter in nighttime Hyytiälä.

Introduction

New particle formation (NPF) contributes significantly to the total atmospheric particle loading (Spracklen *et al.* 2006, Kerminen *et al.* 2012, Lee *et al.* 2013), which in turn affects climate, health, and visibility (IPCC 2013). In addition

to primary sources of aerosols, it is necessary to understand and parametrize the nucleation pathways of secondary aerosol formation from precursor gases in the atmosphere (Kanakidou *et al.* 2005, Kulmala *et al.* 2013, 2014), including the fraction of nucleated particles that subsequently grow to cloud condensation nuclei (CCN) (Mak-

konen *et al.* 2012, Boucher *et al.* 2013, Kulmala *et al.* 2014, Jokinen *et al.* 2015).

Regional NPF events have been observed around the world (e.g. Kulmala *et al.* 2004). A set of physical characteristics allows their systematic identification (e.g. Dal Maso *et al.* 2005, Hirsikko *et al.* 2007): namely, the appearance of nucleation-mode particles (< 25 nm) during the day, and their growth to larger sizes during several hours. Thus, the common practise for identifying NPF events is to analyse a 1-day number size distribution surface plot (Kulmala *et al.* 2012), centered around noon. This highlights the photochemical oxidation pathway needed for NPF to occur.

However, several studies have also reported nighttime new-particle formation. Wiedensohler (1997) observed ultrafine mode (5–15 nm) particles between midnight and early-morning hours downwind of Great Dun Fell, England, in a possible connection to an orographic cloud. A nucleation mode (~5–10 nm) was also detected in the upper troposphere via nocturnal airborne measurements above Colorado, USA (Lee *et al.* 2008) and over the Mediterranean Sea (Rose *et al.* 2015). Suni *et al.* (2008) reported nocturnal aerosol formation in the Eucalyptus forest of Tumbarumba, Australia, with intermediate (1.8–7.5 nm) ions bursts taking place during 32% of the nights they studied. Svenningsson *et al.* (2008) detected multiple nighttime events at cluster ion sizes in a subarctic mire in Abisko, Sweden. Junninen *et al.* (2008) studied four years (2003–2006) of nocturnal ion cluster events (1.3–1.8 nm) from the SMEAR II station in Hyytiälä, Finland, reporting a high event frequency in both polarities, and a higher likelihood for them to appear after a daytime NPF event than after a nonevent. Lehtipalo *et al.* (2011) continued the analysis of Hyytiälä nocturnal events where, in addition to ion clusters, they reported equally frequent neutral sub-3 nm events. They complemented the field data with laboratory experiments, replicating the condensation of low volatile organic vapours from monoterpene precursors to investigate the potential sources of these events. Kalivitis *et al.* (2012) found enhanced nighttime ion concentrations of 1.25–1.66 nm positive and negative ions at Finokalia, Crete, under clean, low condensa-

tion and coagulation sink conditions. Kecorius *et al.* (2015) observed a nighttime 2–10 nm particle concentration increase during ~60% of their July–August 2013 campaign in Beijing, China. Furthermore, Ehn *et al.* (2012) investigated the negative ion mass spectra of nighttime Hyytiälä and concluded that the presence of clusters from highly oxidized, low volatile organics mirrors the signals from α- and β-pinene ozonolysis in their chamber study. Ortega *et al.* (2012) provided experimental results on the oxidation of monoterpenes in dark-chamber conditions, specifically to simulate potential nighttime nucleation as observed by Suni *et al.* (2008). Finally, Peräkylä *et al.* (2014) reported a marked enhancement of ozone-oxidized monoterpene concentrations on the nights prior to a nucleation event, correlating with nucleation mode growth rates during the event of the next morning.

The results of the previous studies motivated us to investigate further the presence of nighttime ion clusters in Hyytiälä, and their possible connection to daytime NPF events. In this study, we investigated 11 years (2003–2013) of negative and positive small and intermediate ion size distributions (0.9–7 nm). Our main goal was to quantify the overall characteristics of nocturnal ion events in Hyytiälä using a long-time series. Particularly, we were interested in assessing how relevant the nocturnal cluster formation might be in terms of its contribution to total new particle formation. The main questions were: (1) Can the formation of ion clusters be distinguished from the constant cluster ion pool? (2) Do the ion clusters activate and grow in size? (3) How do ion concentrations in nighttime ion cluster events compare with those in daytime NPF events, and is there a connection between these two types of events?

Material and methods

Measurement site

All the measurements for this study were conducted during an 11-year period between 20 March 2003 and 31 December 2013 at the Station for Measuring Ecosystem–Atmosphere Relations (SMEAR) II (*see* Hari and Kulmala

2005), in Hyytiälä, southern Finland (61°51´N, 24°17´E; 181 m a.s.l.). The SMEAR II station is located in a boreal pine forest, in a pristine rural environment, ~60 km NE from the nearest city (Tampere). The world's longest, continuous measurements of aerosol particle-number concentrations and size distributions have been carried out there since 1996, along with soil–atmosphere fluxes, sub- and above-canopy fluxes and meteorological variables.

Instrumentation

Ion and particle spectrometers

Mobility size distributions of atmospheric ions were measured at the ground level using a Balancing Scanning Mobility Analyser (BSMA, Tammet 2006). In the BSMA, both negative and positive polarities are alternately scanned in an aspiration-type differential mobility analyzer (DMA) with a mobility range of 3.2–0.032 $cm^2 V^{-1} s^{-1}$, corresponding to 0.8–8 nm in mobility-equivalent Millikan-Fuchs diameter (Mäkelä *et al.* 1996). The BSMA has a 10-min time resolution that includes both polarities.

The classification of days into new particle formation (NPF) events or nonevents was based on the procedure introduced by Dal Maso *et al.* (2005), and was carried out prior to this study using particle number size distribution data from a twin Differential Mobility Particle Sizer (DMPS) system (for apparatus *see* Aalto *et al.* 2001), covering a diameter range of 3–1000 nm (except 3–600 nm during 2003–2004). The DMPS data were also used here as a reference when inspecting the BSMA data.

A Neutral cluster and Air Ion Spectrometer (NAIS; described in Mirme and Mirme 2013) was used to determine the total particle concentration in the 2–3 nm size range. The NAIS consists of two independent DMAs, one for each polarity. Each DMA includes an ion (electrical) filter and corona-needle charger. Along the body of the DMA, 21 collector electrodes measure the current and classify ions according to their electrical mobility. This enables the instrument to classify artificially charged neutral particles in a mobility range of 2.4–0.001 $cm^2 V^{-1} s^{-1}$,

equivalent to 0.9–47 nm of mobility diameter. Data for this instrument were available only for 2006–2013.

Trace gases and meteorological variables

Since 2010, atmospheric trace gas concentrations and meteorological variables have been measured at SMEAR II from different heights (from 4.2 to 74 m) on a mast; as of 2011 the measurements have been made from up to 125 m. The measurements heights we used in this paper were all inside the forest canopy (4.2 and 8.4 m) in order to make a more relevant comparison with the ground-based ion measurements, with the exception of wind direction (measured above the canopy level). NO_x was measured with a chemiluminescence analyzer (TEI 42C TL, Thermo Fisher Scientific); O_3 with an ultraviolet light absorption analyzer (TEI 49C); H_2O, CO_2 and CO with an infrared light absorption analyzer; SO_2 with a fluorescence analyzer (TEI 43 CTL); wind direction (WD) and wind speed (WS) with an ultrasonic anemometer placed above canopy levels; and temperature (T) with a 4-wired PT-100 sensor. Until 2010, relative humidity was calculated using H_2O concentration and T data until 2010, and between 2011 and 2013 it was measured directly using RH sensors (Rotronic Hygromet MP102H with Hygroclip HC2-S3, Rotronic AG). Precipitation was determined from a combination of optical counter signals (FD12P Weather sensor, Vaisala), surface wetness (DRD 11-A raindetector, Vaisala) and rainfall accumulation measured with a tipping bucket counter (Vector Instruments, Rhyl).

Data from all the instruments were available as a long (2003–2013) time series, except for the NAIS data (2006–2013).

Data analysis

Classifying nocturnal events from sub-3 nm ions

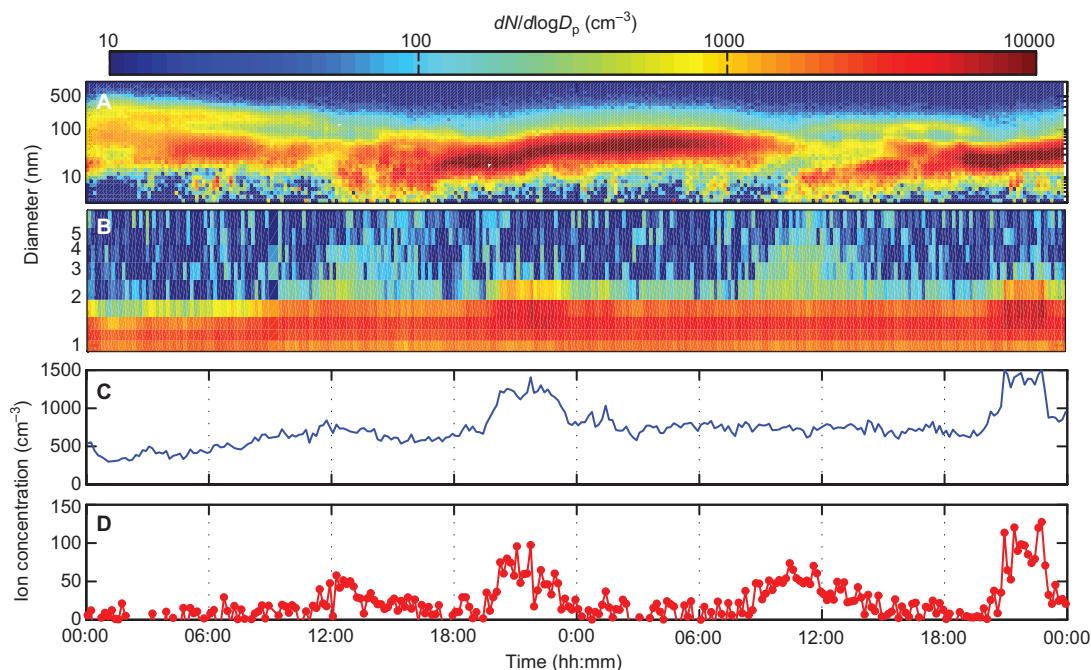Positive and negative ion data measured with the BSMA were analyzed visually by plotting

Fig. 1. Visual classification of a cluster event (CE) on 24–25 April 2013. (**A**) Daytime new particle formation (NPF) events can be seen on Day 1 and Day 2 (DMPS surface plot). Negative CEs in both nights from ~19:00 to midnight (UTC + 2) are seen as (**B**) 'bumps' (BSMA surface plot), and an increase in (**C**) 0.9–3 nm and (**D**) 2–3 nm ion concentrations.

the temporal evolution of ion size distributions during two days (48 h), centered at midnight (local time) between Day 1 and Day 2 (Fig. 1B). The corresponding diurnal 0.9–3 nm ion concentration was plotted in parallel (Fig. 1C). This procedure follows the classification used by Junninen *et al.* (2008) for nocturnal ion clusters (1.3–1.8 nm). Finally, a corresponding particle number size distribution surface plot (hereafter simply 'surface plot') measured by the DMPS (Fig. 1A) was plotted as a reference to daytime NPF classification (event, nonevent or undefined days; Dal Maso *et al.* 2005).

A night between Day 1 and Day 2 was considered to have a sub-3 nm event if the concentration of 0.9–3 nm ions showed a clear increase from its afternoon value, and if there was a distinguishable new 'bump' in the BSMA surface plot. Both these features can be seen in Fig. 1B and C between 19:00 and midnight on both days. A sub-3 nm nonevent was defined as a night when the 0.9–3 nm ion concentration remained low and relatively unchanged from the evening until the next morning (ca. 06:00). Each polarity

was plotted simultaneously, but classified independently. This means, for example, that a given night could have a negative sub-3 nm event and simultaneously a positive ion nonevent. Additionally, the start and end times of the events, as well as the event peak (when the ion concentration reached its maximum value) were manually selected for each polarity from their respective number concentration plots (0.9–3 nm). A nocturnal event date was recorded as the night of Day 1, even if the event began after midnight, which case the starting date was Day 1 and the starting time was 24 hours + hours of Day 2.

Classifying 2–3 nm ion cluster events

Hõrrak *et al.* (1998) and Kulmala *et al.* (2005, 2007, 2013) reported a constant pool of ion- and neutral clusters in the atmosphere, their median size being < 1.8 nm mobility diameter in Hyytiälä (Hirsikko *et al.* 2005, Manninen *et al.* 2009a). Kulmala *et al.* (2013, 2014a) suggested that it is above this constant molecular and small
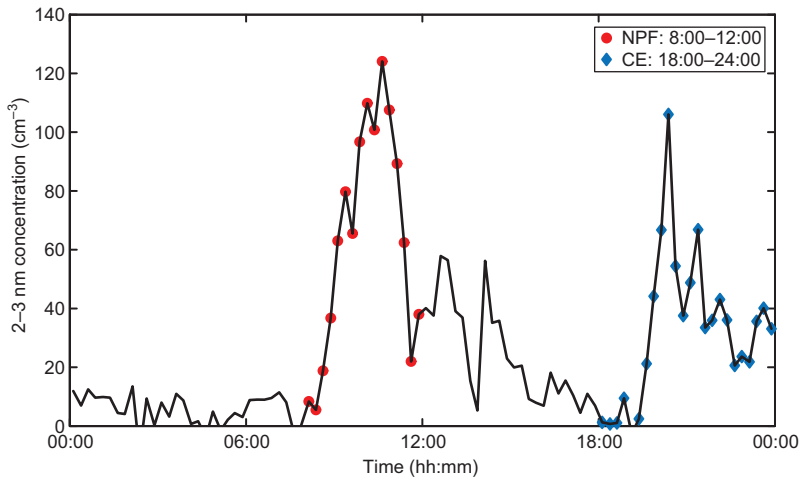
Fig. 2. An example of a 2–3 nm cluster event (CE; 4 May 2003) that passed the ≥ 50 and ≥ 70 cm^{-3} concentration thresholds for 2–3 nm negative ions during the nocturnal time window (18:00–24:00; blue diamonds). The morning NPF event can be seen within the day-time time window (08:00–12:00; red dots).

ions pool, where clusters can be stabilized, activated and undergo enhanced growth. In order to investigate the nocturnal behavior of ions at (or larger than) the critical size for clustering and activation (Yu 2006, Kulmala *et al.* 2013), we re-classified the sub-3 nm nocturnal events based solely on their 2–3 nm ion concentration (illustrated in Fig. 1D), and refer to them as cluster events (CE).

Prior to the re-classification, all evenings with precipitation detected after 15:00 local time (UTC + 2) were discarded from further analysis in order to exclude the effect of rain on intermediate ion production (balloelectric effect, *see* Tammet *et al.* 2009). Additionally, the classification of CE was carried out using one polarity only, namely 2–3 nm negative ions. This choice was made based on the analysis of the sub-3 nm events for both positive and negative ions, which showed little difference between the polarities in terms of event frequency and ion concentrations (*see* Results).

Nighttime 2–3 nm ions

The preliminary list of days with CE was selected automatically from the nocturnal sub-3 nm ion event days with elevated concentrations in the 2–3 nm size range. To begin this selection, a nocturnal time window was defined to be between 18:00 and 24:00 on Day 1, since both the start and peak times of nocturnal sub-3 nm

events occurred during those hours (*see* Results), and CE would be a subsample of those. A similar nocturnal event starting time (~18:00) was reported by Lehtipalo *et al.* (2011) for both ion and neutral nocturnal events in Hyytiälä.

In order to determine when the 2–3 nm ion concentration increase was large enough to be classified as an event, we compared the number of days when the 2–3 nm ions reached concentrations equal to or greater than 50, 70, 90 and 120 cm^{-3} at any point during the 18:00–24:00 time window of Day 1. Based on our analysis in the Result and discussion section "Concentration thresholds for 2–3 nm ion cluster events", we selected the concentration threshold of 70 cm^{-3} to automatically distinguish the 2–3 nm ion cluster events (CE) from the sub-3 nm ion events (*see* Fig. 2 for an example case). After the automatic threshold filter, each CE was visually inspected to confirm the presence of an event from the diurnal ion concentration and surface plots (*see* Fig. 1B and D). Figure 1D illustrates an increase in 2–3 nm ion concentration of ≥ 70 cm^{-3}, comparable to that during the NPF events of Days 1 and 2, and dropping to 0–20 cm^{-3} in-between the events. It is thus a clear example of CE (originally a sub-3 nm event; Fig. 1C). If the 2–3 nm ion concentration fluctuated throughout the day so that a new mode or rise in this concentration did not begin specifically during the nighttime window, the day was discarded from the final selection of CEs.

Daytime versus nighttime conditions

To enable a comparison with daytime NPF events, a similar concentration filter analysis was carried out under an NPF daytime window (between 08:00 and 12:00 local time; Fig. 2 red circles). Previous long-time series analysis of new particle formation in Hyytiälä used a similar time window to study NPF conditions (Nieminen *et al.* 2014, 2015). Specifically in this case, the morning time interval was chosen to capture the beginning of a new particle formation event during which the earliest stages of clustering would occur (~1.7 nm). The NPF event day classification was carried out prior to this study using the conventional methods of Dal Maso *et al.* (2005). In our example case (Fig. 2), the daytime and nighttime time windows satisfactorily contained the NPF and CE events of that day, respectively. To make a fair comparison, only NPF days with 2–3 nm ion concentrations of ≥ 70 cm^{-3} were used in our final analysis (hereafter filtered NPF). For characteristics of each class *see* Table 1.

All the NPF- and CE-nonevent concentrations, as well as trace gases and meteorological parameters are reported here as median values.

Determining the formation rate of 2 nm ions (J_2^-)

Formation rates of negative 2 nm ions (J_2^-,

cm^{-3} s^{-1}) during the cluster events were calculated according to a simplified equation for negatively charged particles given by Kulmala *et al.* (2012):

$$J_2^- = \frac{dN_{2-3}^-}{dt} + \text{CoagS}_{2-3}N_{2-3}^- + \frac{\text{GR}_{<3}}{d_p}N_{2-3}^-, \quad (1)$$
$$+ \alpha N_{2-3}^- N_{<3}^+ - \chi N_{2-3}^- N_{<2}^-$$

The first term on the right-hand side was estimated by calculating the difference in the 2–3 nm ion concentrations (dN_{2-3}^-) between the peak time (t_{max}) and the starting time (t_{start}) of the cluster event, and by dividing it by $dt = t_{max} - t_{start}$ (in s). The remaining variables were estimated as median values for the period $t_{1/2} \pm 10$ min, where $t_{1/2}$ is half way between t_{max} and t_{start}.

The coagulation sink (CoagS_{2-3}; in s^{-1}), i.e., the loss rate of ions due to their coagulation with larger particles, was calculated according to Lehtinen *et al.* (2007) for typical conditions at the SMEAR II station:

$$\text{CoagS}_{dp} = \text{CS}\frac{dp^m}{0.71}, \quad (2)$$

where dp is the diameter of the coagulating particle, and $m = -1.6$ (Lehtinen *et al.* 2007, Kulmala *et al.* 2012). The condensation sink, CS (s^{-1}), in was calculated from the particle number size distribution data measured by DMPS with a 10-min resolution.

The second term on the right-hand side of Eq. 1 includes the ion growth rate ($\text{GR}_{<3}$) and rep-

Table 1. Summary characteristics for each class.

Class	Occurance	Selection criteria
Sub-3 nm nocturnal event	nighttime	Concentration of 0.9–3 nm ions increases distinctly during evening/night hours (~17:00–06:00) and/or a 'bump' or a new mode is seen in BSMA number size surface plot.
Cluster event (CE)	nighttime	No rain after 15:00 hrs (local time). Concentration of 2–3 nm ions increases during 18:00–24:00 of a sub-3 nm nocturnal event day. The 2–3 nm ion concentration reaches ≥ 70 cm^{-3} threshold A clear bump is seen in the BSMA surface plot.
CE nonevent	nighttime	Concentration of sub-3 nm ions remains low and unchanging throughout the night (~17:00–06:00).
Filtered NPF event	daytime	An NPF event day classified as per Dal Maso *et al.* (2005), in which the 2–3 nm ion concentration reaches ≥ 70 cm^{-3} during 08:00–12:00.
NPF nonevent	daytime	A day with no NPF observed, as per Dal Maso *et al.* (2005)
Common nonevent	day-/nighttime	A day with no NPF (as per Dal Maso *et al.* 2005) and no CE present.

resents the growth of 2–3 nm ions above this size range. We observed the lowest CE ion concentration for 3–7 nm ions in the same concentration range as that during nonevents (*see* Results). We thus assumed little growth during CE, and did not take the GR term of Eq. 1 into account.

The fourth term of Eq. 1 represents the loss of 2–3 nm ions via their recombination with sub-3 nm positive ions (concentration $N_{<3}^+$), and the fifth term represents their gain via the attachment of sub-2 nm negative ions ($N_{<2}^-$) with neutral 2–3 nm (N_{2-3}) particles. Following Tammet and Kulmala (2005) and Kulmala *et al.* (2012), the rate coefficients for these processes were taken as $\alpha = 1.6 \times 10^{-6}$ cm^3 s^{-1} and $\chi = 0.01 \times 10^{-6}$ cm^3 s^{-1}. The neutral 2–3 nm particle concentration data needed for the neutral–ion attachment term were available only for 2006–2013. An analysis of the contribution of each term in Eq. 1 showed that the 5th term contributed < 2% to the overall value of J_2^-. For this reason, the decision was made to remove this term from Eq. 1 in order to keep the full 2003–2013 data set in the calculation.

Results

Negative and positive sub-3 nm ion events

During the studied 11 years, sub-3 nm nocturnal events were found in 34% (1324 days) and 30% (1172 days) of the negative and positive ion data, respectively. Both polarities showed similar values in terms of concentrations and event times (Table 2). The events in both polarities had a median starting time of ~19:30, a peak time between 21:30 and 22:00 on Day 1, and an ending time by 04:00 on Day 2. The median sub-3 nm concentrations at the starting time of the events (730 and 800 cm^{-3}) are comparable to the typical ion background levels reported for both polarities in Hyytiälä (Hirsikko *et al.* 2005). Event peak ion concentrations rose considerably, with median levels of 1157 (1168) cm^{-3} for negative (positive) ions, dropping back to background levels (median values: 700 and 765 cm^{-3}) by the end of the events. Compared with positive ions, concentrations of negative ions were slightly lower at the starting and ending times of the events, which is in accordance with the electrode effect (Tuomi 1980) where negative ions are repelled from the Earth's surface, and is noticeable when measuring close to the ground level.

The seasonal distribution of the sub-3 nm ion events was similar for both polarities, with a maximum frequency in May (60% in both polarities, *see* Fig. 3A), and the lowest frequencies during winter (November–February range: 13%–23% for negative and 10%–16% for positive polarities). These features are consistent with the nocturnal cluster ions analysis made by Junninen *et al.* (2008).

Table 2. Characteristics of negative and positive nocturnal sub-3 nm events for the period of 20 Mar. 2003 to 31 Dec. 2013. NPF = new particle formation event. Note that daytime NPF classification (in italics) was carried out with > 3 nm particle data (following Dal Maso *et al.* 2005). * median values with 25th to 75th interquartile range in parentheses.

|	Negative ions	Positive ions
No. of sub-3 nm events (days)	1324	1172
No. of sub-3 nm nonevents (days)	868	976
Start time*	19:25 (18:30–20:52)	19:25 (18:10–20:38)
Peak time*	21:50 (20:10–01:12)	21:35 (20:10–00:43)
End time*	04:20 (01:26–06:43)	04:05 (00:57–06:28)
Start concentration (cm^{-3})	732 (601–858)*	802 (671–913)*
Peak concentration (cm^{-3})	1157 (944–1370)*	1168 (991–1364)*
End concentration (cm^{-3})	700 (570–821)*	765 (639–867)*
Coincident with a *NPF event* (days)	525 (40%)	501 (43%)
Coincident with an *undefined day* (days)	479 (37%)	415 (35%)
Coincident with a *NPF-nonevent* (days)	300 (23%)	238 (20%)
Night before a *NPF event* (days)	504 (38%)	480 (41%)
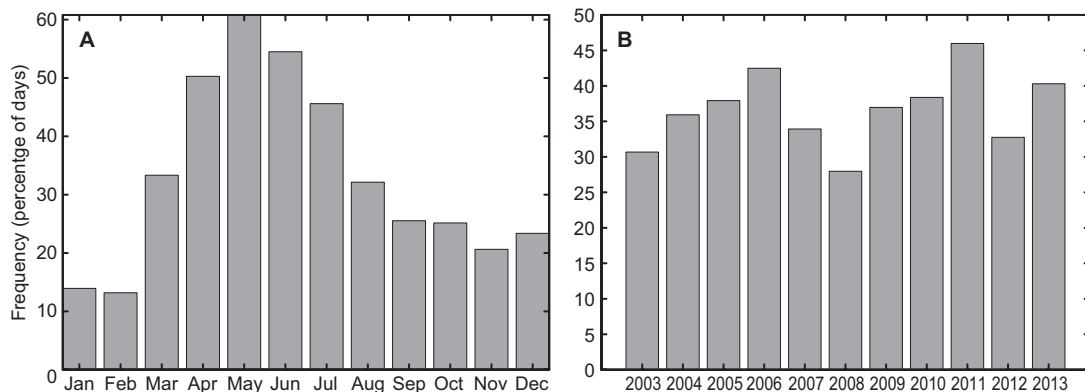
Fig. 3. (**A**) Seasonal and (**B**) yearly frequency of negative cluster events (CE). The frequencies for the positive polarity were similar and are thus not shown. Cluster events peaked in May, with 60% of the month containing CE.

The inter-annual variability of nocturnal sub-3 nm ion events did not show a clear pattern. The lowest event frequency occurred in 2008 (28%), while in the years 2006 (42%) and 2011 (46%) the event fraction was the highest. The observed frequencies of sub-3 nm event nights were quite substantial, and more numerous compared with the 23% frequency of NPF event days in the 16-year time series from Hyytiälä (Nieminen *et al*. 2014). The inter-annual variabilities of the sub-3 nm ion events and NPF events were different, however, as the frequency maxima for NPF events was observed in 2003–2004 and its minimum in 2010, when considering only the years used in this study.

In spite of the different inter-annual variabilities of the sub-3 nm ion and NPF events, ~40% of the sub-3 nm ion events occurred during the evening of a daytime NPF event for both polarities, while ~35% of them occurred during 'undefined' days (unclassified days which nonetheless present similar ambient conditions to NPF, such as RH, CS and solar radiation; *see* Buenrostro Mazon *et al*. 2009). The lowest fraction (~20%) of sub-3 nm event nights occurred on days classified as non-event days. This concurrence of nocturnal ion events with daytime NPF has also been reported by Junninen *et al*. (2008) for Hyytiälä, and by Kalivitis *et al*. (2012) for Finokalia. In order to investigate a possible link or interaction between daytime new particle formation and nighttime clustering, we focused the rest of this study on the 2–3 nm cluster events (CE), a size range relevant to new particle formation.

2–3 nm ion cluster events

Previous studies of nocturnal events in Hyytiälä included ions and particles from the continuously-present cluster pool size range (< 1.8 nm mobility diameter; Hirsikko *et al*. 2005, Kulmala *et al*. 2012, 2013), more specifically 1.3–1.8 nm ions (Junninen *et al*. 2008), and 0.8~3 nm ions and sub-3 nm particles (Lehtipalo *et al*. 2011). In order to investigate whether cluster activation could be observed during the CE nights, the lowest size of the considered ion event was 2 nm. While the contribution of ion-induced nucleation in Hyytiälä has been estimated to be about 10% (Gagné *et al*. 2008, 2010, Manninen *et al*. 2010), the nocturnal events are not limited to ions, as was reported by Lehtipalo *et al*. (2011) with their elevated nocturnal concentration of total sub-3 nm particles. Therefore, CE at 2–3 nm ion diameters and above could serve to indicate the presence of nocturnal NPF in Hyytiälä.

Concentration thresholds for 2–3 nm cluster events

Days with precipitation were removed from further analysis at this stage. This procedure reduced the number of negative sub-3 nm events in the 11-year time series from 1324 (34%) to 985 (25%). Following the analysis of the four concentration thresholds (50, 70, 90 or 120 cm⁻³; *see* Data analysis in Methods), a similar fraction

of CE (8%–45%) and NPF days (9%–52%) were filtered after each concentration threshold (Table 1). Only a small fraction of CE nonevents (3%–14%) and common nonevents (3%–12%) passed each concentration threshold (Table 3).

The 257 CE days obtained after the concentration threshold filter of ≥ 70 cm^{-3} were chosen for further analysis. The reasoning behind this choice was to find a high enough threshold to ensure 'events', while still maintaining a large enough sample size. The threshold ≥ 70 cm^{-3} contained 26% and 33% of the original sub-3 nm nocturnal events and NPF events, respectively, while only 7% of the nonevents passed this filter (Table 3). For comparison, in a study by Leino *et al.* (2016) to automatically identify NPF events from negative ion concentrations, a similar method of thresholds was applied to 2–4 nm negative ions. Leino *et al.* (2016) found that daytime maximum 2–4 nm concentrations surpassed > 50 and > 100 cm^{-3} mostly during days classified as NPF events (> 70%), and to a lesser extent (~20%) when they were undefined and nonevents.

Each of the 257 CE (post-filter ≥ 70 cm^{-3}) was then visually inspected to confirm the presence of a distinct event in the 2–3 nm negative ions, as was done in the original sub-3 nm classification. This resulted in 221 days (86%) classified and verified as CE, indicating that the threshold method was efficient in finding the (2–3 nm) CE from the original post-filtered sample (for examples *see* Fig. 4). The remainder of this study was based on the analysis of these 221 days of CE. For the comparison analysis, the "filtered NPF events" refer to those 295 NPF events (33% of the total NPF days) that were found after applying the ≥ 70 cm^{-3} concentration filter for negative ions. The CE nonevents refer to the 868 nights when no sub-3 nm event had been observed in the original classification; and the common-nonevents refer to the 448 days when there was neither a daytime NPF event nor a nighttime sub-3 nm event.

Characteristics of 2–3 nm ion cluster events

The seasonality of the CE (Fig. 5A) resembled that of the total sub-3 nm events (Fig. 3A), with a minimum in autumn and winter, and a peak from March to August (7%–29%). Similarly, the filtered NPF days (Fig. 5A) had a similar seasonality to that of the original NPF events (Nieminen *et al.* 2014, their Fig. 3), with the exception that the filtered NPF event days peaked in March instead of April. Daily maxima in 2–3 nm ion concentrations during CE were highest in May (Fig. 5B), while the filtered NPF events showed two annual maxima, one in March–April and the other one in September–October (Fig. 5B). Event frequencies and daily concentration maxima thus showed a similar seasonality during CE and NPF days, respectively. By considering potential sources for these clusters to be oxidized organic vapours, it is interesting to note that according to Perakylä *et al.* (2014), the highest monoterpene oxidation capacity associated with ozone in Hyytiälä is in April/May, from noon to early evening. Enhanced monoterpene ozonolysis could be providing condensable oxidized organic vapours not only for daytime, but also under evening conditions.

The median starting time of CE was 18:56 (25th–75th percentiles = 18:15–19:41) local time. This means that CE started typically more than an hour before sunset (Fig. 6), thereby making CE more of an evening rather than strictly a nocturnal

Table 3. Number of days (%) for each class when 2–3 nm ion concentrations reached ≥ 50, 70, 90, and 120 cm^{-3} during any point within its respective daytime (08:00–12:00) or nighttime (18:00–24:00) time windows. CE nonevent = nights when no sub-3 nm event had been observed during the original classification. Common nonevents = days with simultaneously no daytime NPF and no CE in the evening.

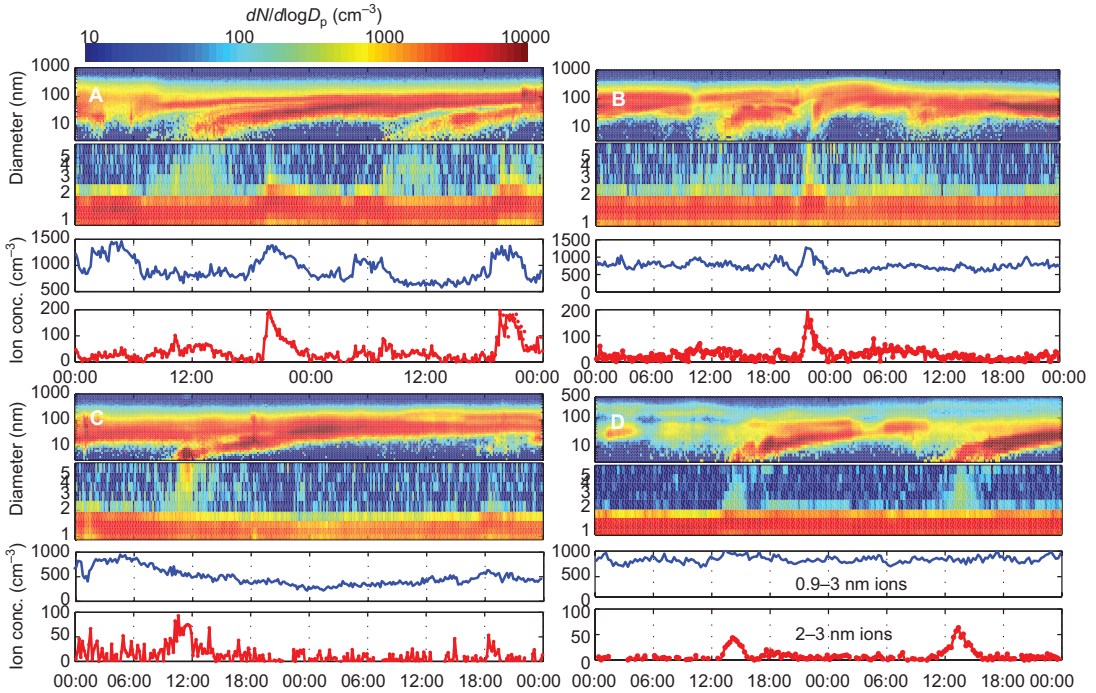| Class (number of days)	≥ 50 cm^{-3}	≥ 70 cm^{-3}	≥ 90 cm^{-3}	≥ 120 cm^{-3}
Sub-3 nm CE (985)	445 (45%)	257 (26%)	163 (17%)	80 (8%)
NPF (894)	461 (52%)	295 (33%)	188 (21%)	83 (9%)
CE nonevent (868)	123 (14%)	60 (7%)	45 (5%)	28 (3%)
Common nonevents (448)	54 (12%)	30 (7%)	25 (6%)	15 (3%)

Fig. 4. Examples of days encountered during the classification of nocturnal events. Each panel displays a set of 48-h plots of number size distributions (DMPS with 3 nm cut-off size, and BSMA) and 0.9–3 nm and 2–3 nm negative ion concentrations. (**A**) Sub-3 nm event (0.9–3 nm) additionally classified as a 2–3 nm cluster event (CE). The sub-3 nm event lasts until the morning of Day 2, with an interruption around midnight, often seen in this class. (**B**) A spike in ion concentration, or 'stick' burst, reaching 7 nm in diameter in the BSMA plot is classified as a sub-3 nm event and a CE. It coincides with what appears as a nighttime 'banana' in the DMPS plot. (**C**) A CE nonevent that proceeds an NPF event. The increase in 2–3 nm ion concentration is seen during the NPF event (~9:00–12:00), after which it decreases and stays constant for the rest of the day. (**D**) An unclassified evening. An increase in ~2 to 2.5 nm ion concentration can be seen on the surface plot but the diurnal ion concentration is unchanging between 18:00 to the following morning. The day was thus left unclassified.
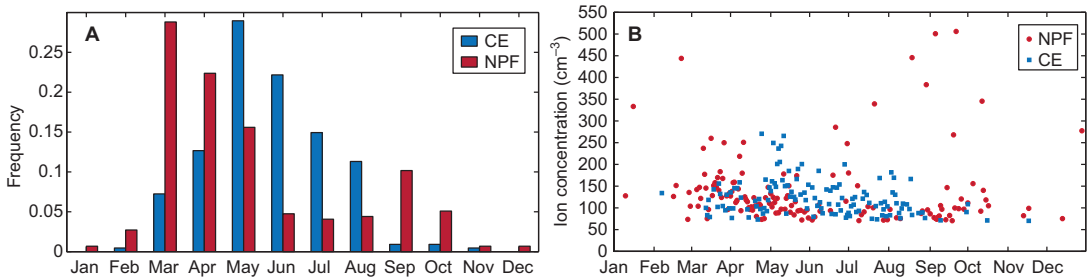

Fig. 5. (**A**) Monthly frequency of days with NPF events and cluster events (CE). (**B**) Maximum daily 2–3 nm ion concentrations during filtered (≥ 70 cm^{-3} ion concentration level) NPF events ($n = 295$) and CE ($n = 221$) within their respective day- and nighttime windows.

phenomenon. The spread of the start times was confined to a relatively narrow band between ca. 18:00–20:00, irrespective of the season. The reason for this feature remains unknown. The median peak time of CE was 20:34 (25th–75th percentiles = 19:46–21:34), around the time of sunset. The nocturnal time-window (18:00–24:00) we chose seemed to satisfactorily contain the start and peak of most of the CEs, as only 17% of CE began before 18:00 ($n = 6$ for 16:30–17:00, $n = $
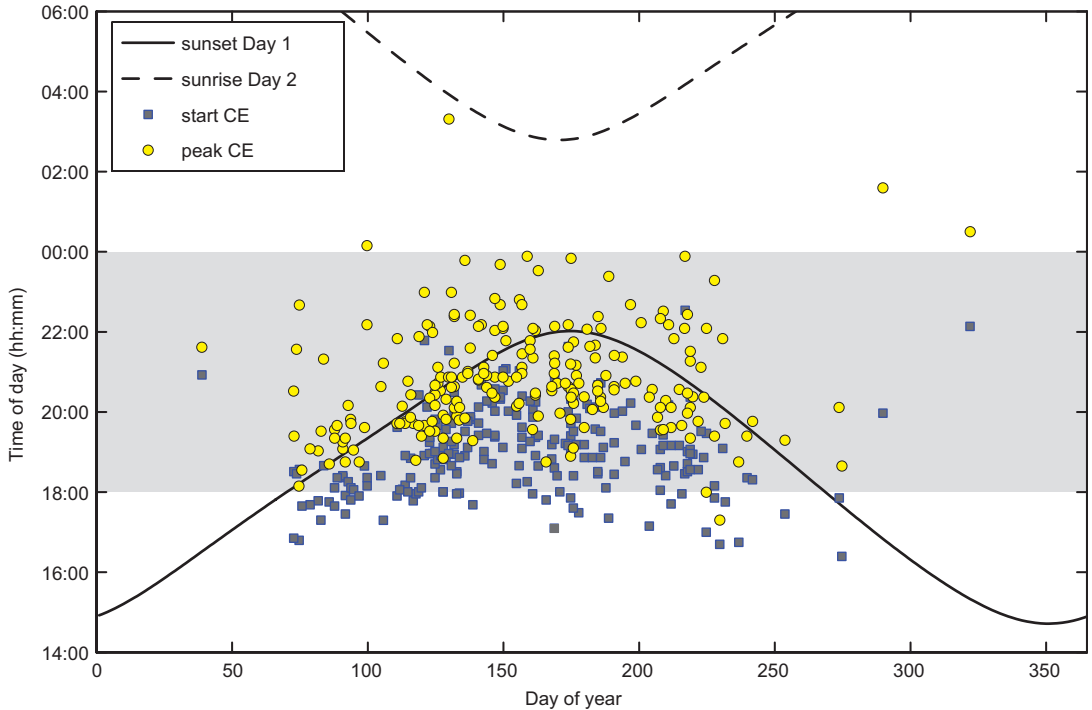
Fig. 6. Sunset and sunrise times for Hyytiälä, Finland. Start times (blue squares) of 2–3 nm CE occur before sunset. CE peak times (yellow circles) occur before and after sunset. Shaded area = nighttime window (18:00–24:00) chosen to analyse CE conditions.

31 for 17:00–18:00 start times), and 2% of them peaked past midnight (24:00 local time).

The median starting and ending concentrations of 2–3 nm ions during CE were ~10 to 15 cm^{-3}, reaching the median value of 96 cm^{-3} during the CE peak time. Kulmala *et al.* (2007) reported 1.8–3 nm ion concentrations reaching ~100 cm^{-3} during an NPF event in Hyytiälä, with nighttime values dropping to < 10 cm^{-3}. In this study (Fig. 5B), maximum ion concentrations during CE were comparable to those during the NPF events. This suggests that during a CE evening the concentration of 2–3 nm ions can rise to the same level as that found during a daytime NPF event, and furthermore at a size range where the cluster activation and growth could be possible (Kulmala *et al.* 2013, 2014).

CE started at ~19:00 local time and ended by midnight of Day 1 (Fig. 7B). The 'bump' in the 2–3 nm size range is evident (*see* Fig. 7B), and the increase in concentration (the 'event') seems to start from the channel below 1.5 nm and fade off shortly after reaching 3 nm. The presence of

a daytime NPF is also apparent on Days 1 and 2, starting at around 09:00 in both BSMA and DMPS surface plots (Fig. 7), illustrating the frequent presence of both CE and NPF events on the same day. Out of the 221 days, 90% of CE were classified as either daytime NPF events (55%) or daytime undefined days (35%) — a higher fraction compared with 77% of the original sub-3 nm nocturnal events (Table 2). Only 10% concurred with daytime nonevent days; a slightly lower percentage (45%) of CEs where followed by an NPF event on Day 2 (Table 4).

In contrast to the sub-3 nm events, CE appear often as quick bursts in the ion concentration (Fig. 7), peaking shortly after their start, with a slower decline thereafter (*see* Fig. 4A). It is interesting that this quick start and gradual decay resembles the simulations done by Ortega *et al.* (2012: fig. 5) for nighttime ozonolysis of monoterpenes. Ortega *et al.* (2012) reproduced experimentally quick bursts events by setting a combination of high ozone and monoterpenes (limonene, α-pinene, and Δ3-carene) concentra-

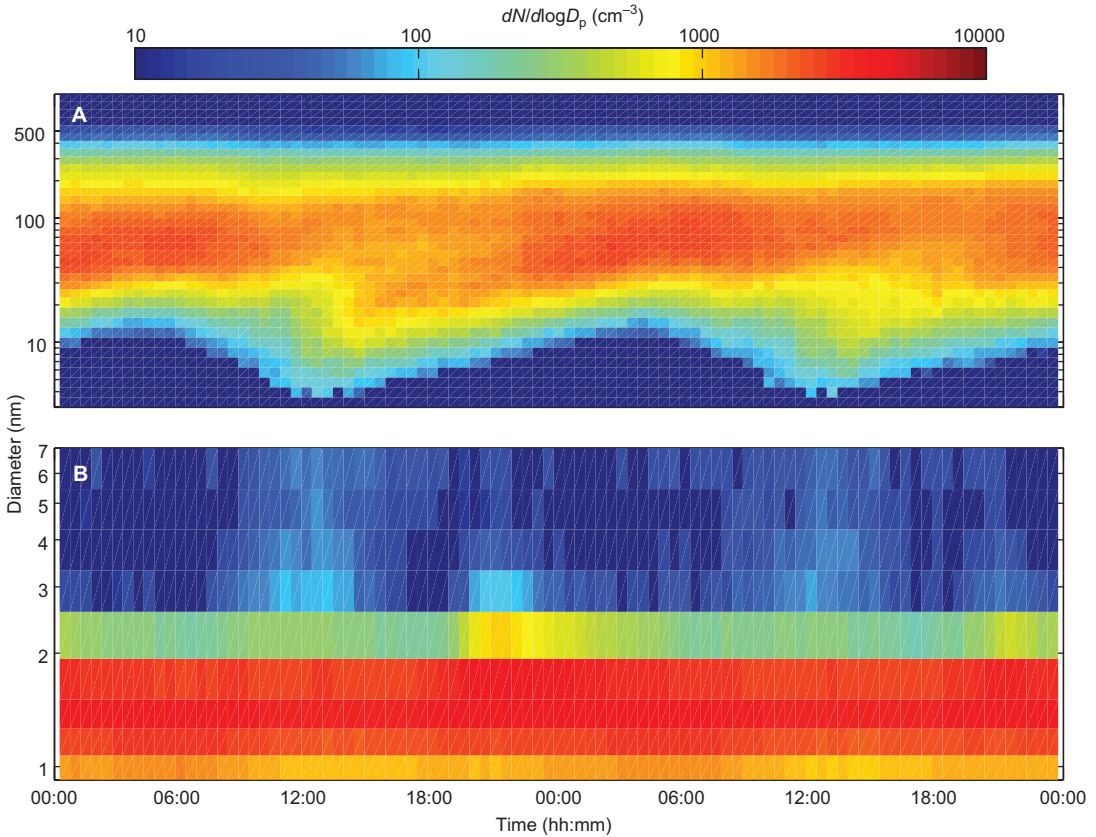**Fig. 7**. The 48-hour median number size distribution surface plots for (**A**) DMPS and (**B**) BSMA data for 2–3 nm CE days. The presence of daytime NPF events seen in both plots, illustrates a coinciding frequency of CEs with NPFs days.

tions that grew into nucleation mode bananas, and suggested that 'hump' events (cut at short sizes) could be locally sourced — and thus limited — events.

Formation rates of negative 2 nm ions

Table 4. Daytime NPF classification based on Dal Maso *et al*. (2005) (using DMPS data) for each of the CE days (Day 1) and the following morning (Day 2).

	CE Day 1 (*n* = 221 days)	CE Day 2 (*n* = 221 days)
NPF day	121 (55%)	100 (45%)
Undefined day	77 (35%)	80 (36%)
Non-event day	23 (10%)	36 (16%)
Bad data day	0	4 (2%)

Ion formation rates (J_2^-) were calculated for 2–3 nm negative CE using Eq. 1. The data needed to calculate the neutral-ion attachment term (NAIS particle mode) were available only for 137 of the 221 CE days (62%). CE had a median J_2^- of 0.12 cm^{-3} s^{-1} (*n* = 210 days) (25th and 75th percentile: 0.09 and 0.14 cm^{-3} s^{-1}). Kulmala *et al*. (2013) reported a median J_2^- value of 0.17 cm^{-3} s^{-1} for negative ions during nucleation events days. While our median J_2^- value is close to that obtained by Kulmala *et al*. (2013), we did not take into account the growth of ions out of the 2–3 nm bin, which has been reported to contribute considerably (~50%) to the calculated ion formation rate (Manninen *et al*. 2009b). Neglecting this loss term in Eq. 1 resulted in a conservative estimate for J_2^- in this study. The largest contribution to Eq. 1 in this study had the ion–ion recombination term (medians: ~65%),

followed by the coagulation sink term (20%) and *dN*/*dt* term (13%).

Daytime and nighttime behaviour of 0.9–7 nm ions

Kulmala *et al.* (2013, 2014) suggested that the sequence of processes from condensable vapors to particle formation can be broken down into clustering, activation of some of these clusters, and subsequent nanoparticle growth, further suggesting that cluster activation takes place at sizes of around 1.5–2 nm. As discussed earlier, CE and daytime NPF events had comparable 2–3 nm ions concentrations.

We compared the concentration of four size bins (0.9–1.5 nm, 1.5–2 nm, 2–3 nm and 3–7 nm) during the daytime and nighttime events/nonevents (Fig. 8). The lowest of these size bins (< 1.5 nm) had the highest ion concentrations in all classes, regardless of whether a CE or filtered NPF event was observed or not, which could be explained by the ubiquitous presence of the cluster ion pool at this size range (Kulmala *et al.* 2004, 2007). The range of ion concentrations in this size bin was not very different between the different types of events/nonevents. In the following 1.5–2 nm size bin, ion concentrations during both day- and nighttime nonevents (median = 18–22 cm^{-3}) were much lower than during CE (235 cm^{-3}) or filtered NPF (96 cm^{-3}) events. Particularly, median 1.5–2 nm ion concentrations during CE were ~2.5 times those during the filtered NPF events. This indicates a build-up of the sub-2 nm ion population during a CE, either due to a higher ion production directly into this size range or due to the growth of ions from the cluster ion pool into this size bin. Suni *et al.* (2008) found a similar nocturnal enhancement of cluster ions (0.3–2 nm) in Tumbarumba, Australia, mentioning radon (Rn) as a possible source of cluster ions. However, in this study, Rn concentration was lower during CE evenings (median = ~0.5 Bq m^{-3}) than in CE nonevents (~1.5 Bq m^{-3}), indicating another source for the ion build-up. The 2–3 nm size bin had very similar ion concentrations between CE and filtered NPF events (median = 31 and 39 cm^{-3}, respectively), as discussed earlier in this paper.

Furthermore, there was as much similarity in the 2–3 nm ion concentration between the CE and filtered NPF events as there was between day- and nighttime nonevents (~1.9 cm^{-3} and 2.6, respectively). While this does not suggest any causality, nor were there chemical analyses available for comparison, it is an interesting observation that both CE and filtered NPF events had similar concentrations during their respective time windows, and common nonevents were scarce in ions of this size throughout the whole day. Ion concentrations in the 3–7 nm size bin, a bin indicative of a clear production of growing nanoparticles, were only substantial during the NPF events (52 cm^{-3}): during CE the concentration was low (9 cm^{-3}) and only slightly higher than those observed during day- and nighttime nonevents (2.6 and 2.1 cm^{-3}, respectively). Overall, the elevated concentrations of 0.9–3 nm ions during both CE and filtered NPF events point toward building up an ion population separate from the cluster ion pool during these events, and particularly so during the CE, yet the growth of ions to larger sizes seems to be efficient only during the NPF events.

To look into more detail if a certain upper limit mobility diameter for CE was distinguishable, we plotted the median diurnal evolution of 1.7–4 nm ion concentrations of the days with CE and days with filtered NPF events (Fig. 9). There was an evident nighttime (18:00–24:00) peak in the median concentration of ions in the 1.7–2.4 nm size range on CE days (8–59 cm^{-3}; Fig. 9B), comparable to or greater than the peak in the concentration of ions of the same ion size on the filtered NPF event days (12–25 cm^{-3}; Fig. 9A). The 2.4–3.0 nm ion concentrations showed a slight evening 'bump' on CE days, but the concentrations remained rather low (~0.3–3 cm^{-3} for each 0.2 nm bin from 2.4–4 nm). Median concentrations of 2.4–3 nm ions on filtered NPF event days were higher (9–11 cm^{-3}), with a rise in concentration around 08:00, coinciding with likely NPF start times. Finally, ion concentrations increased for the largest size bin (3.8–4 nm, dashed line) as well during the NPF events, with a small time lag compared with the lower sizes, indicating the growth of ions from the preceding size bins. We can thus conclude that, on average, the evening
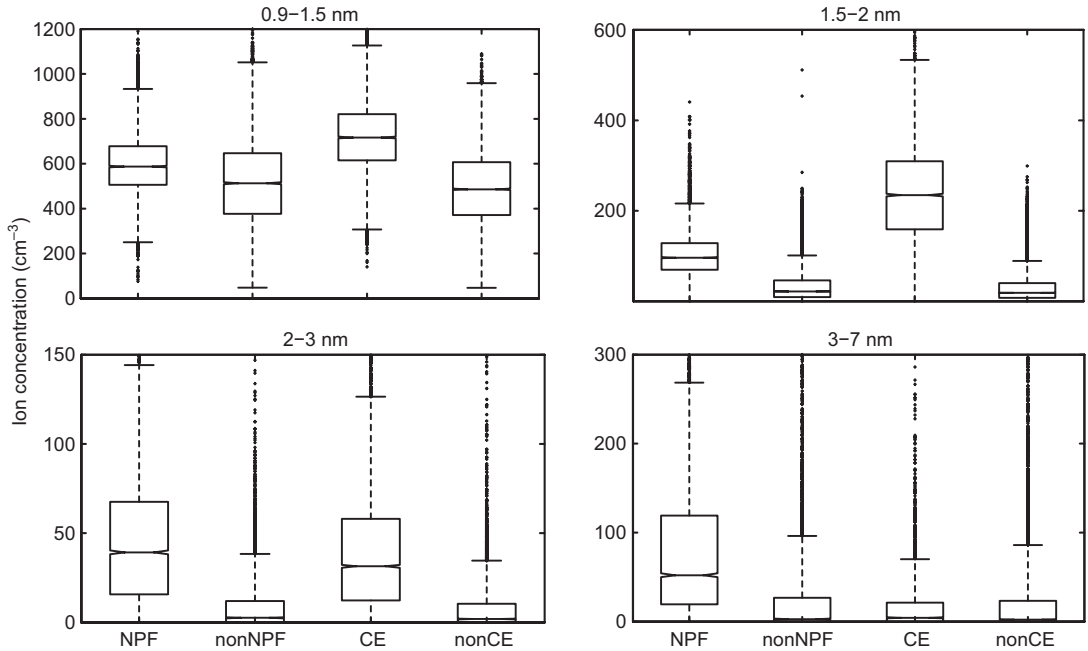
Fig. 8. Ion concentrations of four size bins (0.9–1.5, 1.5–2, 2–3 and 3–7 nm) for NPF and nonNPF daytime (08:00–12:00) as well as CE and nonCE nights (18:00–24:00). The line inside each box is the median; the top and bottom of each box are the 25th and 75th percentiles, respectively; the whiskers are equal to $1.5 \times$ interquartile range, and the points beyond whiskers are outliers ($> 1.5 \times$ interquartile range). The notches visualize variability of the median; if the notches do not overlap the sample medians are different at $p = 0.05$.
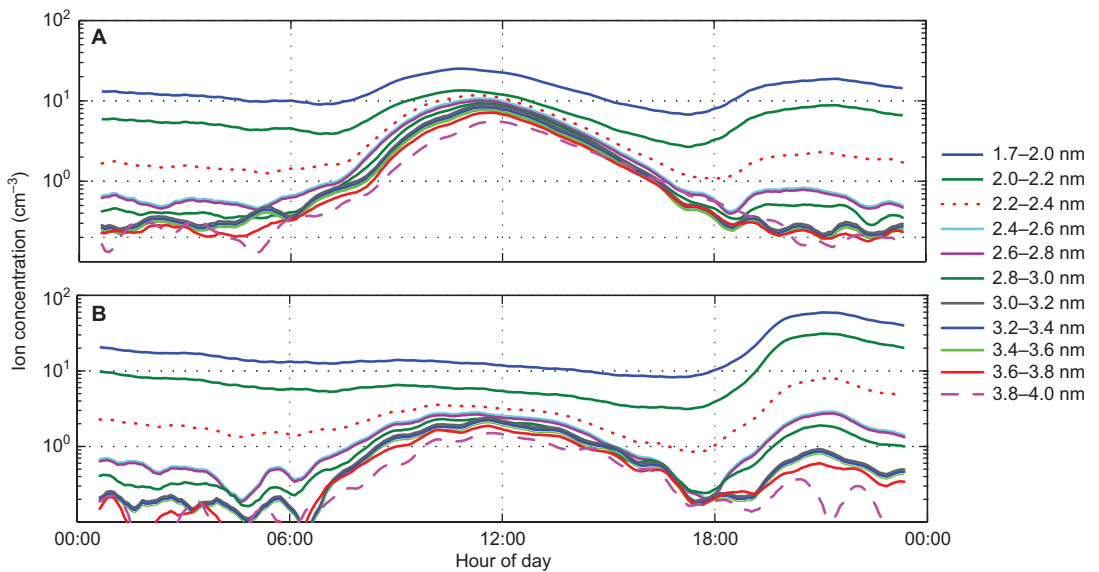

Fig. 9. Median diurnal ion concentrations for 1.7 to 4 nm ion size ranges for (**A**) filtered NPF and (**B**) CE days during the 24-h period (corresponding to Day 1 of CE).

CE are not effectively present past the 2.4 nm size threshold.

Ambient conditions during cluster events

Condensation sink (CS) has been thought to affect atmospheric cluster formation and eventually NPF (Hyvonen *et al.* 2005, Nieminen *et al.* 2014, 2015), since the loss rates of nucleating and condensing vapours, as well as clusters and small particles are directly proportional to CS. In our data set, the median value of CS during spring (March–May) was the lowest during daytime NPF events (1.3×10^{-3} s^{-1}; $n = 196$ days), as compared with evenings with CE (2.3×10^{-3} s^{-1}, $n = 107$ days) and both common daytime (3.1×10^{-3} s^{-1}, $d = 48$ days) and nighttime nonevents (3.2×10^{-3} s^{-1}; $d = 48$ days) (Fig. 10). In summer (June–August), the median value of CS was the highest for CE (3.6×10^{-3} s^{-1}, $n = 100$ days) and somewhat lower for CE nonevents (3.2×10^{-3} s^{-1}, $n = 46$ days) and NPF events (2.0×10^{-3} s^{-1}; $n = 37$ days) (Fig. 10). These features suggest that while high values of CS may supress daytime NPF, and possibly also CE during the spring, it does not seem be limiting the CE taking place in summer.

We observed clear differences in some of the meteorological variables and trace gas concentrations between NPF events, nonevents, CE and CE nonevents during April–May (Fig. 11). To remove the effect of seasonality, only the spring months with the highest frequency of NPF and CE events were presented. Ozone concentration was higher for both NPF (46 ppb) and CE (42 ppb) compared to day- and nighttime nonevents (38 and 35 ppb, respectively), which suggests that ozone could be an important oxidizing agent during nocturnal hours. The preferred wind direction for both CE and NPFs was north-westerly (235°/244° respectively), and the ambient relative humidity was low (45%/42%), in contrast to the nonevent conditions of southeasterly wind directions (~150°–170°) and high RH (80%–90%). The northerly wind sector has previously been associated with clean air masses that are favourable for NPF events (Sogacheva *et al.* 2005). This was further indicated by significantly lower NO$_x$ levels during

NPF and CE. Kalivitis *et al.* (2012) also found a prevalence of clean air mass sectors during their nocturnal ion events, which they further linked to biogenic vapour accumulation as the air passed the island of Crete. Finally, the CE nights were warmer albeit stable (lowest median wind speed), compared with nonevent nights (*see* Fig. 10), as reported by Lehtipalo *et al.* (2011) for the same location. The elevated temperatures could favor higher and longer (lasting into the night) emissions of organic compounds that could then remain undiluted or unadvected due to low wind speeds. Similarities between daytime NPF and evening CE ambient conditions suggest common favorable prevailing conditions for enhanced clustering. This points to the importance of environmental conditions on the role of clustering, and to a lesser extent on the time of day, as nonevents in both day- and nighttime windows differed in ambient conditions from their events counterparts.

Summary and conclusions

Here we report to our knowledge the longest field observations (March 2003–December 2013) of nighttime cluster events. Sub-3 nm nocturnal events (for 0.9–3 nm ions; hereafter 'sub-3 nm events') were observed in both negative and positive polarities during a third of the days during the 11-year time series. In such events, median 0.9–3 nm ion concentrations rose from ~700 cm^{-3} to an event peak of ~1150 cm^{-3} between 19:30 and 04:20 local time (medians). The starting time of the events occurred mostly before sunset, making them more evening events rather than strictly nocturnal events.

In order to investigate the nocturnal behaviour of ions at the critical size for clustering and/or activation (Yu and Turco, 2000, Yu 2006, Enghoff and Svensmark, 2008, Kulmala *et al.* 2013) and subsequent growth, only nighttime events and daytime NPF events with elevated 2–3 nm ion concentrations (≥ 70 cm^{-3}) were filtered and selected for further analysis (hereafter "cluster events" and "filtered NPF events", respectively). Small and intermediate negative ions (0.9–7 nm) concentrations were then compared for day- and nighttime events and nonevents. Sub-2 nm ion concentrations were significantly
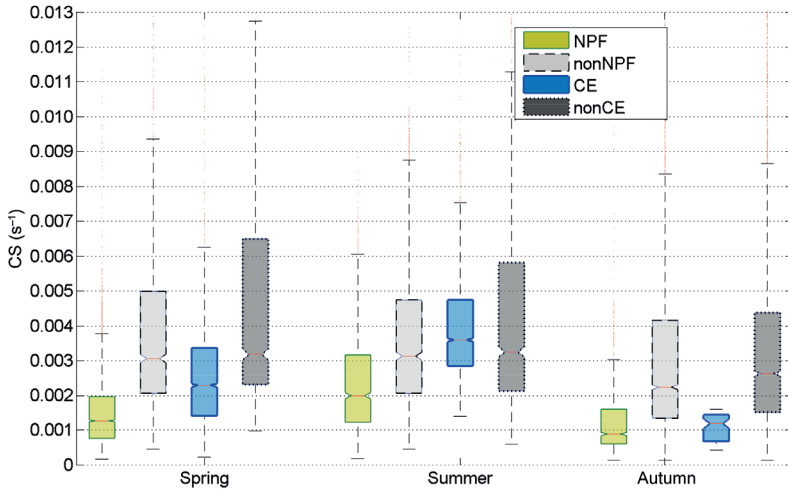
Fig. 10. Seasonal condensation sink (CS) variability for daytime filtered-NPF days (green), CE (blue), and both day-(nonNPF; dashed box) and night (nonCE; dotted box) nonevent classes. Spring = Mar–May, Summer = Jun–Aug, Autumn = Sep–Nov. The line inside each box is the median; the top and bottom of each box are the 25th and 75th percentiles, respectively; the whiskers are equal to 1.5 × interquartile range, and the points beyond whiskers are outliers (> 1.5 × interquartile range). The notches visualize variability of the median; if the notches do not over-lap the sample medians are different at $p = 0.05$.
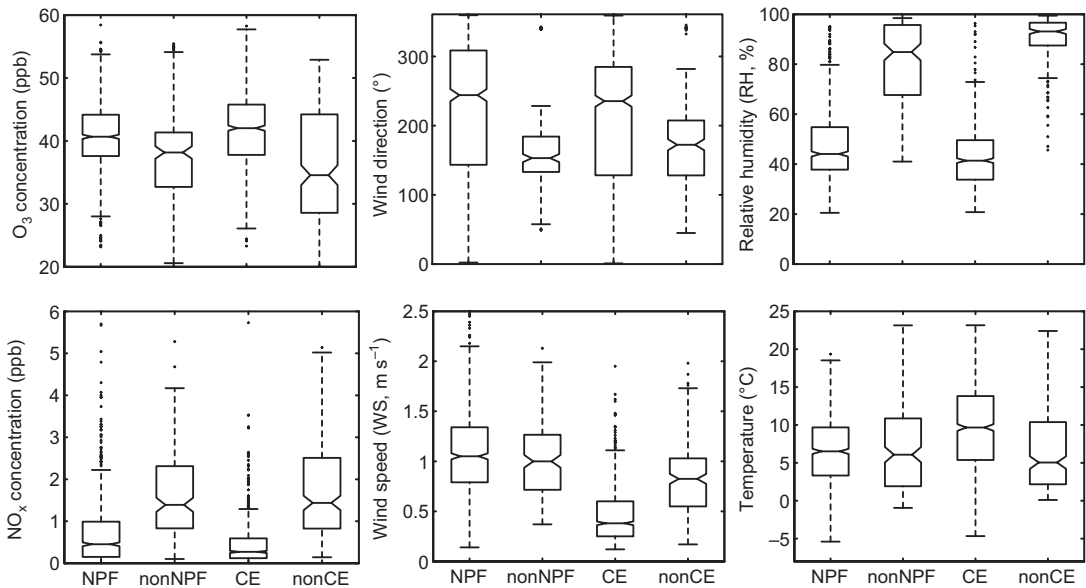

Fig. 11. Meteorological parameters for April–May during NPF and nonNPF daytime (08:00–12:00) as well as CE and nonCE nights (18:00–24:00). The line inside each box is the median; the top and bottom of each box are the 25th and 75th percentiles, respectively; the whiskers are equal to 1.5 × interquartile range, and the points beyond whiskers are outliers (> 1.5 × interquartile range). The notches visualize variability of the median; if the notches do not overlap the sample medians are different at $p = 0.05$.

greater during cluster events (CE) compared with filtered NPF (by a median factor of 2.5), suggesting enhanced clustering (Kulmala *et al.* 2004, 2007) during the nocturnal time window (18:00–24:00). The concentrations of 2–3 nm ions were similar between CE and filtered NPF

events (medians = 31 and 39 cm^{-3}), with a CE median peak concentration of 96 cm^{-3}, similar to the value (~100 cm^{-3}) reported by Kulmala *et al.* (2007) for 1.8–3 nm ion concentrations during NPF events. It must be noted that this size range already falls within the activated cluster size regime proposed by Kulmala *et al.* (2013). However, the largest difference between NPF events and CE was found in the intermediate ions size bin: 3–7 nm ion concentrations increased during NPF (median: 52 cm^{-3}) but remained low (< 10 cm^{-3}) during CE. Specifically, CE ion concentrations decreased substantially at sizes > 2.4 nm, indicating the clusters did not grow above 3 nm. Nonetheless, CE occurred more frequently (~85%) during days with NPF or during undefined days, than during daytime nonevents (~10%). This suggests that the initial steps of clustering may be observable and comparable in both daytime NPF and evening CE, often occurring on the same day. Yet, unlike NPF events, the growth of activated clusters as a last step defining particle formation (Kulmala *et al.* 2014) did not occur in nighttime Hyytiälä. The interesting question is then: why are these CE occurring in the evening, starting around the same time before sunset (~19:00), but not throughout the day? And why do they fail to grow?

With respect to the particle nucleation pathways delineated by Kulmala *et al.* (2013, 2014), it seems CEs achieve clustering, the first step in the gas-to-particle phase transition. Ehn *et al.* (2012) reported highly oxidized organics for nighttime Hyytiälä, which could hint to the possible composition of the CEs. Specifically, CE could be large organic clusters (Schobesberger *et al.* 2013, Ehn *et al.* 2014, Riccobono *et al.* 2014, Praplan *et al.* 2015) that fail to stabilize and grow, perhaps due to the absence of activating vapours (Kulmala *et al.* 2013, 2014), or simply because of their insufficient concentrations as modelled by Ortega *et al.* (2012).

This work provided an alternative window to study the initial stages in new particle formation. The next steps would be to couple neutral and ion clusters to their chemical composition in order to identify a possible formation mechanism. Additionally, the participation of ions in the initial stage of cluster stabilization in new particle formation could be further assessed.

References

Aalto P., Hämeri K., Becker E., Weber R., Salm J., Mäkelä J.M., Hoell C., O'Dowd C.D., Karlsson H., Hansson H.-C., Väkevä M., Koponen I.K., Buzorius G. & Kulmala M. 2001. Physical characterization of aerosol particles during nucleation events. *Tellus* 53B: 344–358.

Boucher O., Randall D., Artaxo P., Bretherton C., Feingold G., Forster P., Kerminen V.-M., Kondo Y., Liao H., Lohmann U., Rasch P., Satheesh S.K., Sherwood S., Stevens B. & Zhang X.Y. 2013. Clouds and aerosols. In: *Climate change 2013: the physical science basis*, Contribution of Working Group I to the Fifth Assessment Report of the Intergovernmental Panel on Climate Change. Cambridge University Press, Cambridge, UK and New York, NY, pp. 571–657.

Buenrostro Mazon S., Riipinen I., Schultz D.M., Valtanen M., Dal Maso M., Sogacheva L., Junninen H., Nieminen T., Kerminen V.-M. & Kulmala M. 2009. Classifying previously undefined days from eleven years of aerosol-particle-size distribution data from the SMEAR II station, Hyytiälä, Finland. *Atmos. Chem. Phys.* 9: 667–676.

Dal Maso M., Kulmala M., Riipinen I., Wagner R., Hussein T., Aalto P.P. & Lehtinen K. E. J. 2005. Formation and growth of fresh atmospheric aerosols: eight years of aerosol size distribution data from SMEAR II, Hyytiälä, Finland. *Boreal Env. Res.* 10: 323–336.

Ehn M., Kleist E., Junninen H., Petäjä T., Lönn G., Schobesberger S., Dal Maso M., Trimborn A., Kulmala M., Worsnop D.R., Wahner A., Wildt J. & Mentel Th.F. 2012. Gas phase formation of extremely oxidized pinene reaction products in chamber and ambient air. *Atmos. Chem. Phys.* 12: 5113–5127.

Ehn M., Thornton J.A., Kleist E., Sipila M., Junninen H., Pullinen I., Springer M., Rubach F., Tillmann R., Lee B., Lopez-Hilfiker F., Andres S., Acir I.-H., Rissanen M., Jokinen T., Schobesberger S., Kangasluoma J., Kontkanen J., Nieminen T., Kurtén T., Nielsen L.B., Jørgensen S., Kjaergaard H.G., Canagaratna M., Maso M. D., Berndt T., Petäjä T., Wahner A., Kerminen V.-M., Kulmala M., Worsnop D.R., Wildt J. & Mentel T.F. 2014. A large source of low-volatility secondary organic aerosol. *Nature* 506: 476–479.

Enghoff M.B. & Svensmark H. 2008. The role of atmospheric ions in aerosol nucleation: a review. *Atmos Chem. Phys.* 8: 4911–4923.

Gagné S., Laakso L., Petäjä T., Kerminen V.-M. & Kulmala M. 2008. Analysis of one year of Ion-DMPS data from the SMEAR II station, Finland. *Tellus* 60B: 318–329.

Gagné S., Nieminen T., Kurtén T., Manninen H.E., Petäjä T., Laakso L., Kerminen V.-M., Boy M. & Kulmala M. 2010. Factors influencing the contribution of ion-induced nucleation in a boreal forest, Finland. *Atmos. Chem. Phys.* 10: 3743–3757.

Hari P. & Kulmala M. 2005. Station for Measuring Ecosystem–Atmosphere Relations (SMEAR II). *Boreal Env. Res.* 10: 315–322.

Hirsikko A., Laakso L., Hõrrak U., Aalto P.P., Kerminen V.-M. & Kulmala M. 2005. Annual and size dependent variation of growth rates and ion concentrations in boreal forest. *Boreal Env. Res.* 10: 357–369.

Hirsikko A., Bergman T., Laakso L., Dal Maso M., Riipinen I., Hõrrak U. & Kulmala M. 2007. Identification and classification of the formation of intermediate ions measured in boreal forest, *Atmos. Chem. Phys.* 7: 201–210.

Hõrrak U., Salm J. & Tammet H. 1998. Bursts of intermediate ions in atmospheric air. *J. Geophys. Res.* 103: 13909–13915.

IPCC 2013. Summary for policymakers. In: Stocker T.F., Qin D., Plattner G.-K., Tignor M., Allen S.K., Boschung J., Nauels A., Xia Y., Bex V. & Midgley P.M. (eds.), *Climate change 2013: the physical science basis. Contribution of Working Group I to the Fifth Assessment Report of the Intergovernmental Panel on Climate Change*, Cambridge University Press, Cambridge, United Kingdom and New York, NY, pp. 3–29.

Jokinen T., Berndt T., Makkonen R., Kerminen V.-M., Junninen H., Paasonen P., Stratmann F., Hermann H., Guenther A., Worsnop D.R., Kulmala M., Ehn M. & Sipilä M. 2015. Production of extremely low volatile organic compounds from biogenic emissions: measured yields and atmospheric implications. *Proc. Natl. Acad. Sci. USA* 112: 7123–7128.

Junninen H., Hulkkonen M., Riipinen I., Nieminen T., Hirsikko A., Suni T., Boy M., Lee S.-H., Vana M., Tammet H., Kerminen V.-M. & Kulmala M. 2008. Observations on nocturnal growth of atmospheric clusters. *Tellus* 60B: 365–371.

Kalivitis N., Stavroulas I., Bougiatioti A., Kouvarakis G., Gagné S., Manninen H.E., Kulmala M. & Mihalopoulos N. 2012. Nighttime enhanced atmospheric ion concentrations in the marine boundary layer. *Atmos. Chem. Phys.* 12: 3627–3638.

Kanakidou M., Seinfeld J.H., Pandis S.N., Barnes I., Dentener F.J., Facchini M.C., Van Dingenen R., Ervens B., Nenes A., Nielsen C.J., Swietlicki E., Putaud J.P., Balkanski Y., Fuzzi S., Horth J., Moortgat G.K., Winterhalter R., Myhre C.E.L., Tsigaridis K., Vignati E., Stephanou E.G. & Wilson J. 2005. Organic aerosol and global climate modelling: a review. *Atmos. Chem. Phys.* 5: 1053–1123.

Kecorius S., Zhang S., Wang Z., Gröss J., Ma N., Wu Z., Ran L., Hu M., Wang P., Ulevicius V. & Wiedensohler A. 2015. Nocturnal aerosol particle formation in the North China Plain. *Lithuanian J. Phys.* 55: 44–53.

Kerminen V.-M., Paramonov M., Anttila T., Riipinen I.,

Fountoukis C., Korhonen H., Asmi E., Laakso L., Lihavainen H., Swietlicki E., Svenningsson B., Asmi A., Pandis S. N., Kulmala M. & Petäjä T. 2012. Cloud condensation nuclei production associated with atmospheric nucleation: a synthesis based on existing literature and new results, *Atmos. Chem. Phys.* 12: 12037–12059.

Kulmala M., Vehkamäki H., Petäjä T., Dal Maso M., Lauri A., Kerminen V.-M., Birmili W. & McMurry P.H. 2004b. Formation and growth rates of ultrafine atmospheric particles: a review of observations. *J. Aerosol Sci.* 35: 143–176.

Kulmala M., Lehtinen K.E.J., Laakso L., Mordas G. & Hämeri K. 2005. On the existence of neutral atmospheric clusters. *Boreal Env. Res.* 10: 79–87.

Kulmala M., Riipinen I., Sipilä M., Manninen H.E., Petäjä T., Junninen H., Maso M.D., Mordas G., Mirme A., Vana M., Hirsikko A., Laakso L., Harrison R.M., Hanson I., Leung C., Lehtinen K.E. & Kerminen V.-M. 2007. Toward direct measurement of atmospheric nucleation, *Science* 318: 89–92.

Kulmala M., Petäjä T., Nieminen T., Sipilä M., Manninen H.E., Lehtipalo K., Dal Maso M., Aalto P.P., Junninen H., Paasonen P., Riipinen I., Lehtinen K.E.J. & Laaksonen A. 2012. Measurement of the nucleation of atmospheric aerosol particles. *Nature Protocols* 7: 1651–1667.

Kulmala M., Kontkanen J., Junninen H., Lehtipalo K., Manninen H. E., Nieminen T., Petäjä T., Sipilä M., Schobesberger S., Rantala P., Franchin A., Jokinen T., Järvinen E., Äijälä M., Kangasluoma J., Hakala J., Aalto P.P., Paasonen P., Mikkilä J., Vanhanen J., Aalto J., Hakola H., Makkonen U., Ruuskanen T., Mauldin R.L.III, Duplissy J., Vehkamäki H., Bäck J., Kortelainen A., Riipinen I., Kurtén T., Johnston M.V., Smith J.N., Ehn M., Mentel T.F., Lehtinen K.E.J., Laaksonen A., Kerminen V.-M. & Worsnop D.R. 2013. Direct observations of atmospheric aerosol nucleation. *Science* 339: 943–946.

Kulmala M., Petäjä T., Ehn M., Thornton J., Sipilä M., Worsnop D.R. & Kerminen V.-M. 2014. Chemistry of atmospheric nucleation: on the recent advances on precursor characterization and atmospheric cluster composition in connection with atmospheric new particle formation. *Annu. Rev. Phys. Chem.* 65: 21–37.

Lee S.-H., Young L.-H., Benson D. R., Suni T., Kulmala M., Junninen H., Campos T.L., Rogers D.C. & Jensen J. 2008. Observations of nighttime new particle formation in the troposphere. *J. Geophys. Res.-Atmos.* 113: D10210, doi:10.1029/2007JD009351.

Lee L.A., Pringle K.J., Reddington C.L., Mann G.W., Stier P., Spracklen D.V., Pierce J.R. & Carslaw K.S. 2013. The magnitude and causes of uncertainty in global model simulations of cloud condensation nuclei. *Atmos. Chem. Phys.* 13: 8879–8914.

Lehtinen K.E.J., Dal Maso M., Kulmala M. & Kerminen V.-M. 2007. Estimating nucleation rates from apparent particle formation rates and vice versa: revised formulation of the Kerminen–Kulmala equation. *J. Aerosol Sci.* 38: 988–994.

Lehtipalo K., Sipilä M., Junninen H., Ehn M., Berndt T., Kajos M.K., Worsnop D.R., Petäjä T. & Kulmala M. 2011. Observations of nano-CN in the nocturnal boreal

forest. *Aerosol Sci. Technol.* 45: 499–509.

Leino K., Nieminen T., Manninen H.E., Petäjä T., Kerminen V.-M. & Kulmala M. 2016: Intermediate ions as a strong indicator for new particle formation bursts in boreal forest. Boreal Env. Res. 21: 274–286.

Mäkelä J.M., Riihelä M., Ukkonen A., Jokinen V. & Keskinen J. 1996. Comparison of mobility equivalent diameter with Kelvin-Thomson diameter using ion mobility data. *J. Chem. Phys.* 105: 1562–1571.

Makkonen R., Asmi A., Kerminen V.-M., Boy M., Arneth A., Guenther A. & Kulmala M. 2012. BVOC-aerosol-climate interactions in the global aerosol-climate model ECHAM5.5-HAM2. *Atmos. Chem. Phys.* 12: 10077–10096.

Manninen H.E., Petäjä T., Asmi E., Riipinen I., Nieminen T., Mikkilä J., Hõrrak U., Mirme A., Mirme S., Laakso L., Kerminen V.-M. & Kulmala M. 2009a. Long-term field measurements of charged and neutral clusters using Neutral cluster and Air Ion Spectrometer (NAIS). *Boreal Env. Res.* 14: 591–605.

Manninen H.E., Nieminen T., Riipinen I., Yli-Juuti T., Gagné S., Asmi E., Aalto P.P., Petäjä T., Kerminen V.-M. & Kulmala M. 2009b. Charged and total particle formation and growth rates during EUCAARI 2007 campaign in Hyytiälä. *Atmos. Chem. Phys.* 9: 4077–4089.

Manninen H.E., Nieminen T., Asmi E., Gagné S., Häkkinen S., Lehtipalo K., Aalto P., Vana M., Mirme A., Mirme S., Hõrrak U., Plass-Dülmer C., Stange G., Kiss G., Hoffer A., Törõ N., Moerman M., Henzing B., de Leeuw G., Brinkenberg M., Kouvarakis G.N., Bougiatioti A., Mihalopoulos N., O'Dowd C., Ceburnis D., Arneth A., Svenningsson B., Swietlicki E., Tarozzi L., Decesari S., Facchini M. C., Birmili W., Sonntag A., Wiedensohler A., Boulon J., Sellegri K., Laj P., Gysel M., Bukowiecki N., Weingartner E., Wehrle G., Laaksonen A., Hamed A., Joutsensaari J., Petäjä T., Kerminen V.-M. & Kulmala M. 2010. EUCAARI ion spectrometer measurements at 12 European sites — analysis if new particle formation events. *Atmos. Chem. Phys.* 10: 7907–7927.

Manninen H.E., Schobesberger S., Hirsikko A., Hakala J., Skromulis A., Kangasluoma J., Ehn M., Junninen H., Mirme A., Mirme S., Sipilä M., Petäjä T., Worsnop D. R. & Kulmala M. 2011. Characterisation of corona-generated ions used in a Neutral cluster and Air Ion Spectrometer (NAIS). *Atmos. Meas. Tech. Discuss.* 4: 2099–2125.

Mirme S. & Mirme A. 2013. The mathematical principles and design of the NAIS — a spectrometer for the measurement of cluster ion and nanometer aerosol size distributions. *Atmos. Meas. Tech.* 6: 1061–1071.

Nieminen T., Yli-Juuti T., Manninen H.E., Petäjä T., Kerminen V.-M. & Kulmala M. 2015. Technical note: New particle formation event forecasts during PEGASOS–Zeppelin Northern mission 2013 in Hyytiälä, Finland. *Atmos. Chem. Phys.* 15: 12385–12396.

Nieminen T., Asmi A., Dal Maso M., Aalto P. P., Keronen P., Petäjä T., Kulmala M. & Kerminen V.-M. 2014. Trends in atmospheric new particle formation: 16 years of observations in boreal forest environment. *Boreal Env. Res.* 19 (suppl. B): 191–214.

Ortega I.K., Suni T., Boy M., Grönholm T., Manninen H.E., Nieminen T., Ehn M., Junninen H., Hakola H., Hellén H., Valmari T., Arvela H., Zegelin S., Hughes D., Kitchen M., Cleugh H., Worsnop D. R., Kulmala M. & Kerminen V.-M. 2012. New insights into nocturnal nucleation, *Atmos. Chem. Phys.* 12: 4297–4312.

Peräkylä O., Vogt M., Tikkanen O.-P., Laurila T., Kajos M. K., Rantala P. A., Patokoski J., Aalto J., Yli-Juuti T., Ehn M., Sipilä M., Paasonen P., Rissanen M., Nieminen T., Taipale R., Keronen P., Lappalainen H.K., Ruuskanen T.M., Rinne J., Kerminen V.-M., Kulmala M., Bäck J. & Petäjä T. 2014. Monoterpenes' oxidation capacity and rate over a boreal forest: temporal variation and connection to growth of newly formed particles. *Boreal Env. Res.* 19 (suppl. B): 293–310.

Praplan A.P., Schobesberger S., Bianchi F., Rissanen M.P., Ehn M., Jokinen T., Junninen H., Adamov A., Amorim A., Dommen J., Duplissy J., Hakala J., Hansel A., Heinritzi M., Kangasluoma J., Kirkby J., Krapf M., Kürten A., Lehtipalo K., Riccobono F., Rondo L., Sarnela N., Simon M., Tome A., Tröstl J., Winkler P.M., Williamson C., Ye P., Curtius J., Baltensperger U., Donahue N.M., Kulmala M. & Worsnop D.R. 2015. Elemental composition and clustering behaviour of alpha-pinene oxidation products for different oxidation conditions. *Atmos. Chem. Phys.* 15: 4145–4159.

Riccobono F., Schobesberger S., Scott C.E., Dommen J., Ortega I.K., Rondo, L., Almeida, J., Amorim, A., Bianchi, F., Breitenlechner, M., David, A., Downard, A., Dunne, E.M., Duplissy, J., Ehrhart, S., Flagan, R.C., Franchin, A., Hansel, A., Junninen, H., Kajos, M., Keskinen, H., Kupc, A., Kürten, A., Kvashin, A.N., Laaksonen, A., Lehtipalo, K., Makhmutov, V., Mathot, S., Nieminen, T., Onnela, A., Petäjä, T., Praplan, A.P., Santos, F.D., Schallhart, S., Seinfeld, J.H., Sipilä, M., Spracklen, D.V., Stozhkov, Y., Stratmann, F., Tomé, A., Tsagkogeorgas, G., Vaattovaara, P., Viisanen, Y., Vrtala, A., Wagner, P.E., Weingartner, E., Wex, H., Wimmer, D., Carslaw, K.S., Curtius, J., Donahue, N.M., Kirkby, J., Kulmala, M., Worsnop, D.R. & Baltensperger U. 2014. Oxidation products of biogenic emissions contribute to nucleation of atmospheric particles. *Science* 344: 717–721.

Rose, C., Sellegri, K., Freney, E., Dupuy, R., Colomb, A., Pichon, J.-M., Ribeiro, M., Bourianne, T., Burnet, F. & Schwarzenboeck, A. 2015. Airborne measurements of new particle formation in the free troposphere above the Mediterranean Sea during the HYMEX campaign, *Atmos. Chem. Phys.* 15: 10203–10218.

Schobesberger S., Junninen H., Bianchi F., Lönn G., Ehn M., Lehtipalo K., Dommen J., Ehrhart S., Ortega I.K., Franchin A., Nieminen T., Riccobono F., Hutterli M., Duplissy J., Almeida J., Amorim A., Breitenlechner M., Downard A.J., Dunne E.M., Flagan R.C., Kajos M., Keskinen H., Kirkby J., Kupc A., Kürten A., Kurtén T., Laaksonen A., Mathot S., Onnela A., Praplan A. P., Rondo L., Santos F.D., Schallhart S., Schnitzhofer R., Sipilä M., Tomé A., Tsagkogeorgas G., Vehkamäki H., Wimmer D., Baltensperger U., Carslaw K. S., Curtius J., Hansel A., Petäjä T., Kulmala M., Donahue N.M. & Worsnop D.R. 2013. Molecular understanding of atmo-

spheric particle formation from sulfuric acid and large oxidized organic molecules. *Proc. Natl. Acad. Sci. USA* 110: 17223–17228.

Sogacheva L., Dal Maso M., Kerminen V.-M. & Kulmala M. 2005. Probability of nucleation events and aerosol particle concentration in different air mass types arriving at Hyytiälä, southern Finland, based on back trajectory analysis. *Boreal Env. Res.* 10: 479–491.

Spracklen D.V., Carslaw K.S., Kulmala M., Kerminen V.-M., Mann G.W. & Sihto S.-L. 2006. The contribution of boundary layer nucleation events to total particle concentrations on regional and global scales, *Atmos. Chem. Phys.* 6: 5631–5648.

Suni T. Kulmala M., Hirsikko A., Bergman T., Laakso L., Aalto P.P., Leuning R., Cleugh H., Zegelin S., Hughes D., van Gorsel E., Kitchen M., Vana M., Hõrrak U., Mirme S., Mirme A., Sevanto S., Twining J. & Tadros C. 2008. Formation and characteristics of ions and charged aerosol particles in a native Australian Eucalypt forest. *Atmos. Chem. Phys.* 8: 129–139.

Svenningsson B., Arneth A., Hayward S., Holst T., Massling A., Swietlicki E., Hirsikko A., Junninen H., Riipinen I., Vana M., Dal Maso M., Hussein T. & Kulmala M. 2008. Aerosol particle formation events and analysis of high

growth rates observed above a subarctic wetland–forest mosaic. *Tellus* 60B: 353–364.

Tammet H. & Kulmala M. 2005. Simulation tool for atmospheric aerosol nucleation bursts. *J. Aerosol Sci.* 36: 173–196.

Tammet H. 2006. Continuous scanning of the mobility and size distribution of charged clusters and nanometer particles in atmospheric air and the Balanced Scanning Mobility Analyzer, BSMA. *Atmos. Res.* 82: 523–535.

Tammet H., Horrak U. & Kulmala M. 2009. Negatively charged nanoparticles produced by splashing of water. *Atmos. Chem. Phys.* 9: 357–367.

Tuomi T. 1980. Atmospheric electrode effect: approximate theory and wintertime observations. *PAGEOPH* 119: 31–45.

Wiedensohler A. 1997. Nighttime formation and occurrence of new particles associated with orographic clouds. *Atmos. Environ.* 31: 2545–2559

Yu F. & Turco R.P. 2000. Ultrafine aerosol formation via ion-mediated nucleation. *Geophys. Res. Lett.* 27: 883–886.

Yu F. 2006. From molecular clusters to nanoparticles: second-generation ion-mediated nucleation model *Atmos. Chem. Phys.* 6: 5193–5211.